

is a natural consequence of the longitude of observation, and the spreading by Keplerian shear explains also why they all appear concentric. In the second study, several clumps were tracked around Saturn, indicating a full 90-km range in semimajor axes (with a standard deviation of 45 km). The observations reported here show that the strands, organized as a rotating spiral, have a wider range of semimajor axes (300 km); however, it may be possible that the tracked clumps were only the brightest ones, naturally located closer to the core in the spiral model.

By the end of 2009, Prometheus and the F ring will be in a close-encounter configuration because of the precession of their orbits resulting from Saturn's oblateness (2, 8). It is very probable that additional spirals will then

be created by Prometheus and could be observed in an extended Cassini mission.

References and Notes

1. B. A. Smith *et al.*, *Science* **212**, 163 (1981).
2. C. D. Murray, M. K. Gordon, S. M. G. Winter, *Icarus* **129**, 304 (1997).
3. M. R. Showalter, *Icarus* **171**, 356 (2004).
4. A. S. Bosh, C. B. Olkin, R. G. French, P. D. Nicholson, *Icarus* **157**, 57 (2002).
5. C. C. Porco *et al.*, *Science* **307**, 1226 (2005).
6. P. D. Nicholson *et al.*, *Science* **272**, 509 (1996).
7. M. R. Showalter, J. A. Burns, *Icarus* **52**, 526 (1982).
8. C. D. Murray, S. M. G. Winter, *Nature* **380**, 139 (1996).
9. C. D. Murray *et al.*, *Nature* **437**, 1326 (2005).
10. J. A. Burns, D. P. Hamilton, M. R. Showalter, in *Interplanetary Dust*, E. Grün, B. A. S. Gustafson, S. F. Dermott, H. Fechtig, Eds. (Springer-Verlag, Berlin, 2001), pp. 641–725.
11. M. R. Showalter, *Science* **282**, 1099 (1998).
12. M. R. Showalter, J. B. Pollack, M. E. Ockert, L. Doyle, J. B. Dalton, *Icarus* **100**, 394 (1992).
13. D. P. Hamilton, J. A. Burns, *Nature* **365**, 498 (1993).

14. M. C. Lewis, G. R. Stewart, *Astron. J.* **120**, 3295 (2000).
15. S. F. Dermott, *Nature* **290**, 454 (1981).
16. R. A. Kolvoord, J. A. Burns, M. R. Showalter, *Nature* **345**, 695 (1990).
17. J. Hänninen, *Icarus* **103**, 104 (1993).
18. C. C. Porco *et al.*, *IAU Circ.* **8432**, 1 (2004).
19. J. N. Spitale, unpublished data.
20. F. Poulet, B. Sicardy, P. D. Nicholson, E. Karkoschka, J. Caldwell, *Icarus* **144**, 135 (2000).
21. We thank H. Throop, J. Cuzzi, J. Decriem, C. Ferrari, M. Hedman, C. Murray, P. Nicholson, M. Tiscareno, and three anonymous referees for useful comments and discussions. We also acknowledge the work of the CICLOPS operations group in making the observations described here possible.

Supporting Online Material

www.sciencemag.org/cgi/content/full/310/5752/1300/DC1

Table S1

Figs. S1 to S3

26 August 2005; accepted 19 October 2005
10.1126/science.1119387

REPORTS

Encoding Electronic Properties by Synthesis of Axial Modulation-Doped Silicon Nanowires

Chen Yang,^{1*} Zhaohui Zhong,^{1*} Charles M. Lieber^{1,2,†}

We describe the successful synthesis of modulation-doped silicon nanowires by achieving pure axial elongation without radial overcoating during the growth process. Scanning gate microscopy shows that the key properties of the modulated structures—including the number, size, and period of the differentially doped regions—are defined in a controllable manner during synthesis, and moreover, that feature sizes to less than 50 nanometers are possible. Electronic devices fabricated with designed modulation-doped nanowire structures demonstrate their potential for lithography-independent address decoders and tunable, coupled quantum dots in which changes in electronic properties are encoded by synthesis rather than created by conventional lithography-based techniques.

A wide range of nanoscale electronic and photonic devices have been made with carbon nanotube and nanowire functional elements (1–4). Although the nanomaterials are important for achieving observed functional properties in these nanodevices, many of the most critical features have been defined with the use of similar lithographic approaches that drive and ultimately limit the planar semiconductor industry. The current dependence on lithography thus could reduce advantages of these nanoscale elements in proposed applications and suggests that nonlithographic approaches

for encoding key features or information are needed.

Modulation of the composition has been demonstrated recently in relatively simple nanorod and nanowire structures to yield functional structures (5–8). For example, gold grown on the tips of cadmium selenide nanorods provides specific points for self-assembly and electrical contact (5). Modulation of the dopant or composition of nanowires during synthesis also has been used to define functional *p*-type/*n*-type diodes (6) and single quantum dots (8). These studies show the potential for synthesis to define function without lithography, yet the level of information and function encoded in the materials has been very limited. We now describe selective dopant modulation during the growth of silicon nanowires with essentially complete control over the

size, spacing, and number of modulated regions.

Applications of nanowires in conventional electronics could be facilitated by using synthesis to define the aspects of transistors that are currently enabled by lithographic and ion-beam processing, such as feature uniformity and controlled doping. For example, the high sensitivity of carbon nanotubes to adsorbed gases and solid coatings, along with lithographic patterning, has been exploited in transistor structures (9, 10). Greater ease of circuit assembly could be afforded by the ability to create semiconductor nanowires that are uniform in shape and that can be doped selectively along their length, in that the formation of regions with different electronic properties would be intrinsic to nanowire synthesis and would not require intermediate lithographic patterning and/or electrical contacts. Many of the wiring steps normally created by lithography can be encoded by varying the doping sequence of the nanowires so that the only postfabrication lithographic steps would be those involved in making external input and output contacts to individual nanowires.

Synthesis of dopant-modulated nanowire structures in which function can be predicted on the basis of the encoded axial sequence of doping is challenging: It requires effectively pure axial or one-dimensional (1D) growth without simultaneous radial or 2D growth (Fig. 1A), because even a few atomic layers of dopant deposited on the surface of a nanowire can dominate its overall electronic properties (11). In the metal nanocluster-catalyzed vapor-liquid-solid growth process (3–5), which has been widely used to prepare nanowires, the dopant must be added exclusively at the nanocluster catalyst without reaction and deposition at the much larger area of the exposed solid

¹Department of Chemistry and Chemical Biology,

²Division of Engineering and Applied Sciences, Harvard University, Cambridge, MA 02138, USA.

*These authors contributed equally to this work.

†To whom correspondence should be addressed.
E-mail: cml@cmliris.harvard.edu

surface of the growing nanowire in order to encode electronic function. Simultaneous radial growth with axial elongation, which would obscure modulation of electronic properties along the nanowire axis, is likely more common than recognized (11) and is apparent in extreme cases as visible tapering seen in nanowire structures.

In nanocluster-catalyzed growth of Si nanowires with silane as a reactant, homogeneous gas-phase decomposition produces reactive species that can lead to uncontrolled and deleterious radial overcoating of the nanowire during elongation (11, 12). To control

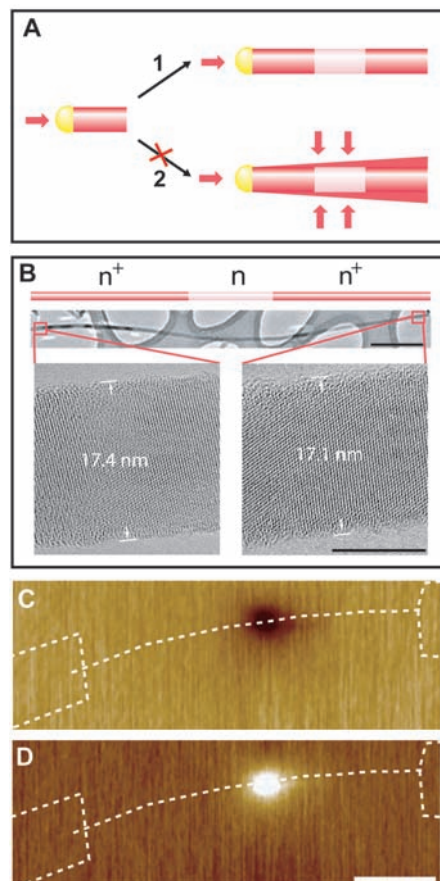


Fig. 1. Synthesis and characterization of modulation-doped nanowires. (A) Illustrations of (1) pure axial and (2) simultaneous axial and radial growth occurring during gold nanocluster (yellow) catalyzed nanowire synthesis. Simultaneous radial growth (2) leads to undesirable deposition of high dopant concentration material over the entire nanowire. (B) (Top) Schematic and low-resolution TEM image of a representative n^+-n-n^+ modulation-doped silicon nanowire. Scale bar, 500 nm. (Bottom) High-resolution TEM images recorded at the two ends indicated by red boxes. Scale bar, 10 nm. (C and D) SGM images of a n^+-n-n^+ modulation-doped nanowire recorded with a $V_{\text{tip}} = -9$ V and $+9$ V, respectively, and $V_{\text{sd}} = 1$ V. The dark and bright regions correspond to reduced and enhanced conductance, respectively. The white dashed lines highlight the positions of source-drain electrodes and nanowire. Scale bar, 1 μm .

radial deposition down to the atomic level, we used a local substrate heater (versus a tube furnace reactor) and carried out growth in a H_2 atmosphere (13), which suppresses the decomposition of silane and inhibits deposition on the nanowire surface (14, 15). Transmission electron microscopy (TEM) studies of modulation-doped n^+-n-n^+ silicon nanowires (Fig. 1B), where n^+ and n represent the heavily and lightly n -type regions, respectively, show that the nanowires prepared in this way have uniform diameters for lengths of >10 μm . High-resolution TEM analysis of the opposite ends of a representative n^+-n-n^+ silicon nanowire (Fig. 1B) further demonstrate that the diameters are 17.4 and 17.1 nm. This 0.3-nm variation is on the order of a single atomic layer and shows that radial overcoating has been effectively eliminated during growth of these modulation-doped structures.

To determine whether the n^+-n-n^+ nanowires exhibit expected variations in the elec-

tronic properties associated with modulated dopant concentration, we used scanning gate microscopy (SGM) (6, 13, 16). In these measurements, a conducting atomic force microscopy probe with an applied voltage (V_{tip}) functions as a spatially localized gate, which enables the conductance of the nanowire with fabricated source and drain contacts to be varied and mapped (13). Data acquired from a n^+-n-n^+ nanowire device with a 555-nm-long n -type segment (length based on growth time) exhibits localized variations in conductance between the source and drain (Fig. 1, C and D). When $V_{\text{tip}} = -9$ V the conductance of this region is reduced, and when $V_{\text{tip}} = +9$ V the conductance is enhanced. The changes in conductance are consistent with the expected depletion or accumulation of carriers in the lightly doped n -type region, and moreover, the ~ 525 -nm length of this region agrees well with that expected of 555 nm. No SGM response was observed from other regions of the nanowire, and is consistent with heavily doped n^+ regions connected to the source and drain in the n^+-n-n^+ device. These data thus confirm that our synthetic approach yields spatially and electrically well defined n^+-n-n^+ nanowire structures.

We explored limits to these modulated nanowires by preparing and characterizing structures of the general form $n^+-(n-n^+)_N$, where N is the number of repeat units. Representative SGM data (Fig. 2, A to C) show that N and the repeat spacing can be varied over a wide range. Specifically, the SGM results show $n^+-(n-n^+)_N$ modulated structures with $N = 3, 6,$ and 8 and repeat spacings of 3.20, 1.55, and 0.75 μm , respectively. The observed number of repeats and spacing between repeats agrees well with that designed through synthesis (3.12, 1.56, and 0.78 μm , respectively).

To further explore the synthetic control of these modulated structures, we also prepared structures with variable repeat lengths, where the separation between fixed-length n -type segments is varied by the n^+ growth time. The SGM data show that the designed $N = 5$ structure has separations of 0.80, 1.15, 1.85, and 3.43 μm , which are consistent with the variation in growth times (Fig. 2D). These data and measurements from a number of additional samples (>15) have been summarized as a plot of $n-n^+$ length versus growth time (Fig. 2E) and demonstrate the linear dependence that is essential for predictable dopant modulation during synthesis.

The potential for scaling $n-n^+$ features to smaller sizes was also probed by reducing the nanowire growth rate. We found that the growth rate decreased linearly to ~ 2.9 nm/s when the pressure was reduced from 320 to 80 torr (Fig. 2F). Notably, reproducible $N = 3$ structures prepared at 160 and 80 torr exhibited average repeat spacings of 180 nm

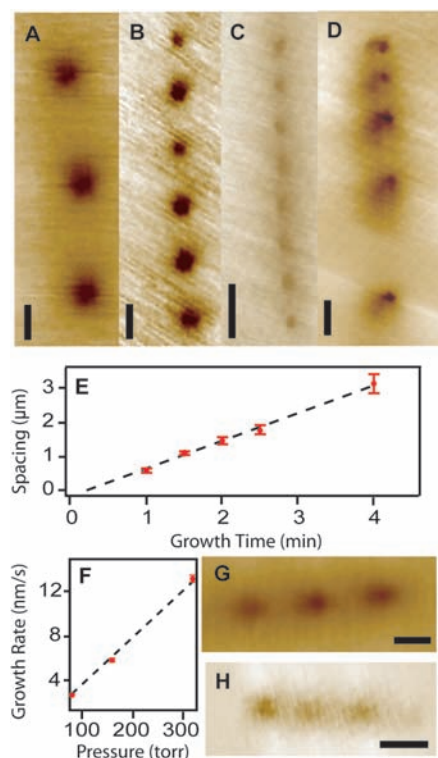


Fig. 2. Scalable synthesis of modulation-doped nanowires. SGM images of $n^+-(n-n^+)_N$ nanowires where (A) $N = 3$, (B) $N = 6$, and (C) $N = 8$, and the growth times for the n/n^+ regions are 1/3, 1/1, and 0.5/0.5 min, respectively. (D) SGM image of $N = 5$ nanowire, where the growth time for the n regions is 0.5 min, and n^+ sections are 0.5, 1, 2, and 4 min. Scale bars, 1 μm . (E) Repeat spacing versus growth time at total pressure of 320 torr. (F) Growth rate versus growth pressure. SGM images of $n^+-(n-n^+)_3$ modulation-doped nanowires synthesized with total pressures of (G) 160 torr and (H) 80 torr. The growth time for each n and n^+ region is 15 s. Scale bars, 100 nm. Error bars in (E) and (F) show means \pm SD.

(Fig. 2G) and 90 nm (Fig. 2H), respectively, where the average section length in each structure was only 90 and 45 nm, respectively. These values do not represent a lower limit of the feature size. Because dopant diffusion is negligible at the growth temperature (17), it should be possible to reduce the feature size to at least that of the diameter of the nanowire (6), which for molecular-scale Si nanowires (18) is 3 to 5 nm.

The substantial differences in nanowire conductance resulting from locally gating n and n^+ segments can be used as a general method for addressing individual nanowires in an array when the nanowires have different n/n^+ sequences or codes. To test this idea, we first fabricated n^+-n-n^+ Si nanowire transistors with three equally spaced top metal gates (Fig. 3A). The nanowire tran-

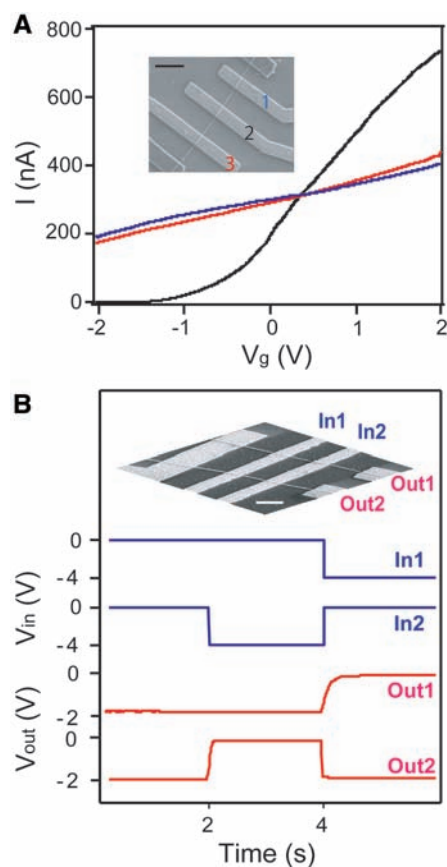


Fig. 3. Modulation-doped address decoder. (A) I versus V_g ($V_{sd} = 1$ V) measured for an n^+-n-n^+ silicon nanowire device, where gates 1, 2, and 3 (inset) correspond to blue, black, and red curves, respectively. The native silicon oxide was used as a gate dielectric with Au metal gates. (Inset) Scanning electron microscopy (SEM) image of the device. Scale bar, 1 μm . (B) SEM image of a 2-by-2 decoder configured using two modulation-doped silicon nanowires as outputs (Out1 and Out2) and two Au metal gates, which were deposited over a uniform Si_3N_4 dielectric as inputs (In1 and In2). Scale bar, 1 μm . Plots of input (blue) and output (red) voltages for the 2-by-2 decoder. Supply voltage is -2 V.

sistor is easily turned off by gate 2 (-1 V), whereas the other gates produce only small conductance changes. Because the three gates are fabricated at the same time in a parallel process, the observed address selectivity is intrinsic to the differences in dopant concentration of n and n^+ sections of the Si nanowire and is distinct from lithographically defined steps previously used (19) to create differential responses in a specific nanowire region.

We have extended this basic approach to arrays (Fig. 3B). Two metal top gates, In1 and In2, were deposited directly on two modulation-doped silicon nanowires configured as outputs, Out1 and Out2. Conductance versus applied gate voltage (V_g) data measured at the four cross points show that Out1 and Out2 can only be turned off by In1 and In2, respectively (fig. S1), and thus, these inputs can selectively address Out1 and Out2 (Fig. 3B); that is, the array functions as an address decoder circuit for multiplexing and demultiplexing signals. A key point in our approach is that lithography is only used to define a regular array of microscale gate wires and is not needed to create a specific address code at the nanoscale as in previous work (19). Because synthesis is used to define the code required for nanoscale addressing (not lithography), we call this a “lithography-independent” addressing scheme. In the demonstration example of Fig.

3B, we took advantage of stochastic end-to-end nanowire alignment to produce distinct codes from a single type of nanowire. Indeed, the general case of a stochastic addressing with modulation-doped nanowires has been analyzed and shown to be an efficient approach for addressing dense nanoscale arrays; that is, it requires $\sim 2.2\ln(N)$ nanowires for addressing N lines when N is large (20).

Control of the size and separation of modulation-doped regions also enables synthesis to define quantum dot (QD) structures, in which the Fermi level offset caused by variations in dopant concentration produces potential barriers confining the QD (Fig. 4A). Conductance versus V_g and bias voltage (V_{sd}) studies of $n^+-n-n_{\text{QD}}^+-n-n^+$ modulation-doped silicon nanowires—in which the lightly doped n -type regions define barriers for a variable length QD, n_{QD}^+ —reveal well-defined diamond structures (Fig. 4B); the single-period diamond shows that transport occurs through a single QD structure (21). Notably, the geometry-dependent gate capacitance, C_g , determined from these data, 23.5 aF, agrees well with the value, 24.1 aF, calculated from the ~ 500 -nm QD size determined by SGM imaging (Fig. 4B, inset). In addition, current (I) versus V_g data for this nanowire and a structure in which the n_{QD}^+ section is reduced by half to ~ 250 nm (Fig. 4C) show single-

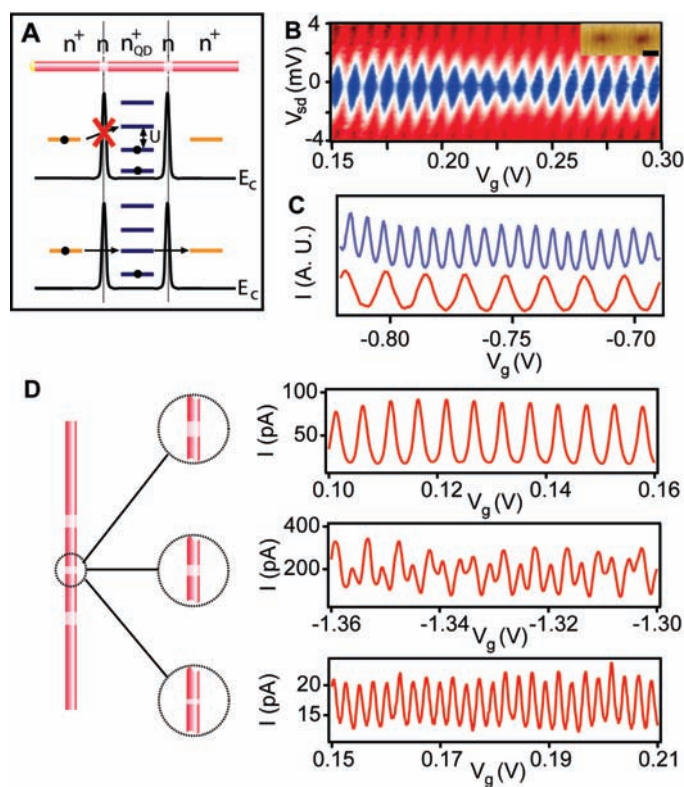


Fig. 4. QD structures defined by synthesis. (A) Schematic of n^+ QD structure confined by two n -type barriers within a modulation-doped nanowire. The conduction band (E_c) offset of the n^+ and n sections induce tunneling barriers with Coulomb blockade phenomenon observed when thermal energy is $\ll U$, the charging energy (21). The red X indicates blockage of charge transport. (B) Plot of $\partial I/\partial V_{sd}$ versus V_{sd} and V_g recorded at 1.5 K on a $n^+-n-n_{\text{QD}}^+-n-n^+$ device. The blue regions correspond to low values of $\partial I/\partial V_{sd}$, and the red regions correspond to high values; the red color corresponds to 1.8 μS . The middle n_{QD}^+ and two n sections were grown for 3 and 0.5 min, respectively, at 80 torr. (Inset) SGM image of the same device.

Scale bar, 200 nm. (C) $I - V_g$ data taken at 1.5 K on the device in (B) (blue curve) and another device with the n_{QD}^+ section grown for 1.5 min (red curve). $V_{sd} = 0.2$ mV. A.U., arbitrary units. (D) Coupled double-QD structure with variable-width n_2 section between the two QDs. (Right) $I - V_g$ data recorded at 1.5 K on three devices with n_2 sections grown for 15, 10, and 5 s (top to bottom).

period oscillations in both devices, although the period ΔV_g is approximately doubled in the 250- versus 500-nm QD. Because ΔV_g is inversely proportional to the gate capacitance, $\Delta V_g = e/C_g$, and QD size, this comparison shows that the true size of the confined QD can be controlled in a predictable manner in these modulation-doped nanowires (22).

The potential of our approach for encoding coupled quantum structures has been explored in modulation-doped silicon nanowires that have structures of the form $n^+-n_1-n_{\text{QD}}^+-n_2-n_{\text{QD}}^+-n_1-n^+$, where n_1 are fixed-width tunnel barriers that weakly couple the structure to source and drain electrodes, and n_2 is a variable-width barrier that couples the two QDs (Fig. 4D, left panel). The $I - V_g$ data recorded from representative nanowire devices with three different n_2 barrier widths coupling the QDs (Fig. 4D, right panel) demonstrate several key points. First, the device with the largest barrier exhibits a single Coulomb oscillation period that yields a capacitance consistent with the size of each individual QD determined from SGM measurements. This result shows qualitatively that the two QDs are weakly coupled, and moreover, have sizes that are similar. Second, the data from the device with an intermediate-width n_2 barrier exhibits a splitting of each of the Coulomb oscillation peaks into doublets, which is the signature of enhanced tunneling conductance between the QDs (23, 24). This observation agrees with previous studies (23, 25, 26) where coupled dots were defined by lithographically patterned gate electrodes. Last, as the barrier width is reduced further, a single Coulomb oscillation period is again observed, although the capacitance shows that the effective QD size is twice that of the individual n_{QD}^+ regions; that is, the structures are fully delocalized.

These studies demonstrate the ability to synthesize coupled QDs within nanowires, where the interaction between quantum structures is defined by synthesis not lithography. More generally, this work demonstrates the potential of encoding functional information into nanostructures during synthesis, which we believe will open up opportunities for conventional and quantum electronic devices and circuits in the future.

Reference and Notes

1. P. L. McEuen, M. S. Fuhrer, H. Park, *IEEE Trans. Nanotechnology* **1**, 78 (2002).
2. H. Dai, *Acc. Chem. Res.* **35**, 1035 (2002).
3. C. M. Lieber, *Mater. Res. Soc. Bull.* **28**, 486 (2003).
4. L. Samuelson et al., *Phys. E* **25**, 313 (2004).
5. T. Mokari, E. Rothenberg, I. Popov, R. Costi, U. Banin, *Science* **304**, 1787 (2004).
6. M. S. Gudixsen, L. J. Lauhon, J. Wang, D. C. Smith, C. M. Lieber, *Nature* **415**, 617 (2002).
7. M. T. Bjork et al., *Appl. Phys. Lett.* **80**, 1058 (2002).
8. M. T. Bjork et al., *Nano Lett.* **4**, 1621 (2004).
9. C. Zhou, J. Kong, E. Yenilmez, H. Dai, *Science* **290**, 1552 (2000).
10. V. Derycke, R. Martel, J. Appenzeller, Ph. Avouris, *Nano Lett.* **1**, 453 (2001).

11. A. B. Greytak, L. J. Lauhon, M. S. Gudixsen, C. M. Lieber, *Appl. Phys. Lett.* **84**, 4176 (2004).
12. L. J. Lauhon, M. S. Gudixsen, D. Wang, C. M. Lieber, *Nature* **420**, 57 (2002).
13. Materials and methods are available as supporting material on Science Online.
14. J. M. Jasinski, S. M. Gates, *Acc. Chem. Res.* **24**, 9 (1991).
15. R. T. White, R. L. Espino-Rios, D. S. Rogers, M. A. Ring, H. E. O'Neal, *Int. J. Chem. Kinet.* **17**, 1029 (1985).
16. A. Bachtold et al., *Phys. Rev. Lett.* **84**, 6082 (2000).
17. P. M. Fahey, P. B. Griffin, J. D. Plummer, *Rev. Mod. Phys.* **61**, 289 (1989).
18. Y. Wu et al., *Nano Lett.* **4**, 433 (2004).
19. Z. Zhong, D. Wang, Y. Cui, M. W. Bockrath, C. M. Lieber, *Science* **302**, 1377 (2003).
20. A. DeHon, P. Lincoln, J. E. Savage, *IEEE Trans. Nanotechnology* **2**, 165 (2003).
21. L. P. Kouwenhoven et al., in *Proceedings of Advanced Study Institute on Mesoscopic Electron Transport*, L. L. Sohn, L. P. Kouwenhoven, G. Schön, Eds. (Kluwer, Dordrecht, Netherlands, 1997).
22. Recent studies have demonstrated the formation of single quantum dots in InP/InAs composition-modulated nanowires, where InP is used to produce confining barriers for an InAs QD (8).
23. F. R. Waugh et al., *Phys. Rev. B* **53**, 1413 (1996).
24. The tunneling conductance for the strongly coupled QDs was estimated to be $0.9 G_0$, where $G_0 = 2e^2/h$, e is the elementary charge, and h is Planck's constant, assuming that interdot capacitance is negligible compared with individual QD capacitances (23).
25. N. Mason, M. J. Biercuk, C. M. Marcus, *Science* **303**, 655 (2004).
26. C. Fasth, A. Fuhrer, M. T. Bjork, L. Samuelson, *Nano Lett.* **5**, 1487 (2005).
27. We thank H. Park and A. DeHon for discussion. C.M.L. acknowledges support of this work by the Defense Advanced Research Projects Agency.

Supporting Online Material

www.sciencemag.org/cgi/content/full/310/5752/1304/DC1
Materials and Methods
Fig. S1

12 August 2005; accepted 24 October 2005
10.1126/science.1118798

Super-Compressible Foamlike Carbon Nanotube Films

Anyuan Cao,^{1*} Pamela L. Dickrell,² W. Gregory Sawyer,² Mehrdad N. Ghasemi-Nejhad,¹ Pulickel M. Ajayan^{3*}

We report that freestanding films of vertically aligned carbon nanotubes exhibit super-compressible foamlike behavior. Under compression, the nanotubes collectively form zigzag buckles that can fully unfold to their original length upon load release. Compared with conventional low-density flexible foams, the nanotube films show much higher compressive strength, recovery rate, and sag factor, and the open-cell nature of the nanotube arrays gives excellent breathability. The nanotube films present a class of open-cell foam structures, consisting of well-arranged one-dimensional units (nanotube struts). The lightweight, highly resilient nanotube films may be useful as compliant and energy-absorbing coatings.

Structural foams (1, 2) have a variety of applications in modern society such as in construction, energy dissipation, cushioning, and packaging. Mechanical strength (compressive stress) and compressibility (strain) are two important factors that determine the performance and applications of foams; however, these two properties are of opposing nature. Increasing the volume of the cells (i.e., the void area) in a foam results in higher compressibility (up to 75%) but causes rapidly decreasing strength (2–4). For the foam at a fixed chemical composition, its modulus (E_f) decreases with increasing relative cell volume (ϕ) as $E_f = CE(1 - \phi)^2$, where C is a constant (close to unity) and E is the cell edge

modulus (1). Metallic (e.g., Al) foams have higher compressive strength than polymeric foams, but the plastic deformation of cell structures results in little resilience upon load release (5). The elastic segments (struts) between adjacent cells form the architecture of a foam, and it is the bending and buckling of these struts that allows the foam to be compressed; the property of a strut (determined by its composition, geometry, and dimension) dictates the compressive behavior (6, 7).

A carbon nanotube (8, 9) is perhaps the best strut to make ultralight yet strong foams, considering its exceptional mechanical strength, low density, and high elasticity (10). In particular, the nanotube exhibits extreme structural flexibility (10–12) and can be repeatedly bent through large angles and strains without structural failure (13). The ability of nanotubes to adopt and switch between various buckled morphologies makes them capable of accommodating and sustaining large local strains while maintaining structural integrity (14, 15).

We show that vertically aligned nanotubes (16) form a highly resilient open-cell

¹Department of Mechanical Engineering, University of Hawaii at Manoa, Honolulu, HI 96822, USA. ²Department of Mechanical and Aerospace Engineering, University of Florida, Gainesville, FL 32611, USA. ³Department of Materials Science and Engineering, Rensselaer Polytechnic Institute, Troy, NY 12180, USA.

*To whom correspondence should be addressed. E-mail: anyuan@hawaii.edu (A.C.); ajayan@rpi.edu (P.M.A.)